Journal of Food Engineering 368 (2024) 111913

Contents lists available at ScienceDirect

Journal of Food Engineering

journal homepage: www.elsevier.com/locate/jfoodeng

Modeling the extraction of espresso components as dispersed flow through a packed bed

Mauricio Vaca Guerra [a,*], Yogesh M. Harshe [b], Lennart Fries [b], James Payan Lozada [a], Aitor Atxutegi [a], Stefan Palzer [d], Stefan Heinrich [a]

[a] Institute of Solids Process Engineering and Particle Technology, Hamburg University of Technology, Denickestraße 15, 21073 Hamburg, Germany
[b] Nestlé Research, Route du Jorat 57, CH-1000 Lausanne 26, Switzerland
[d] Nestlé S.A. Avenue Nestlé 55 CH-1800 Vevey, Switzerland

ARTICLE INFO

Keywords:
Espresso extraction
Espresso components
Packed bed
Dispersive flow
Mass transfer coefficient
Kinetics modeling

ABSTRACT

Espresso extraction involves a flow of heated water through a densely packed bed of porous particles driven by high pressure. This flow is impacted by a series of structural changes that the packed bed undergoes during water percolation. In this work, we aim to improve and extend an existing extraction model from Moroney et al. (2015) by integrating the axial dispersive flow through the coffee bed via a characteristic axial diffusion coefficient. This parameter was obtained by means of tracer pulse experiments applied to different packed bed configurations at different stages of the extraction. Increasing axial dispersion of the flow was observed experimentally with progressing extraction time. This characteristic was included in the model by considering a transition of the axial diffusion coefficients from the initial filling phase to the steady-state flow phase. The model was also extended to describe the concentration of individual species in the brew. Lumped mass transfer coefficients and saturation concentrations were fitted to experimental results. The model was then validated against experimental data from extraction trials using different particle size distributions. Good agreement was found for the extracted total dissolved solids as well as for the concentrations of caffeine, trigonelline and 5-caffeoylquinic acid (5-CQA). The proposed approach enables an estimation of the overall and individual component concentrations for various particle size ranges while accounting for the dynamic internal changes inside the packed bed during the extraction time.

1. Introduction

Espresso, as a variety of coffee beverage preparations, has become one of the most popular beverages in the world. Around 3 billion cups are consumed every day with an increasing trend(International Coffee Organization, 2021) . That is why, a large incentive has emerged to optimize the amount of coffee used per brew. In the end, this translates into optimal extraction conditions and less raw material needed per cup, thus a CO_2 footprint reduction. An effective way to achieve a clear understanding of the physical mechanisms involved in the process is by means of relatively simple mathematical models where the main process parameters are identified. However, the espresso extraction as a mass transfer process inside a densely packed bed of porous particles, is a complex food matrix system with several intercorrelated parameters through a considerably extended range of size scales (Fries, 2021). Several authors have proposed mathematical models to describe the extraction process by separating coffee grounds in two main groups of particles, a coarse fraction (>100 μm) and a fines fraction (<100 μm) (Anderson et al., 2003; Wang et al., 2016). Further research has demonstrated that coffee particle size is a critical parameter for the extraction process, since it determines both the flow conditions around particles in the packed bed and the limiting diffusion resistance of compounds from internal particle pores (Spiro and Selwood, 1984; Schenker et al., 2000).

Due to the convection-diffusion nature of espresso extraction mass transfer, the relevance of the advective flow through the bed becomes evident; however, the dynamic nature of the packed bed permeability complicates the accurate description of this process. Studies have been elaborated on the correlation between particle size distribution and permeability of the bed (Corrochano et al., 2015; Vaca Guerra et al., 2023b), other studies have focused on simulating the macroscopic phenomena occurring during percolation like fines migration, erosion

* Corresponding author.
E-mail address: mauricio.vaca@tuhh.de (M. Vaca Guerra).

https://doi.org/10.1016/j.jfoodeng.2023.111913
Received 4 September 2023; Received in revised form 20 November 2023; Accepted 23 December 2023
Available online 26 December 2023

(Mo et al., 2021) and particle swelling (Mo et al., 2022) to predict the final steady-state volume flow and the respective extraction rate from coffee. Ellero et al. (2019) formulated an espresso extraction simulation based on the Smoothed Particle Hydrodynamics (SPH) where the impact of the fines migration on the transient nature of the volume flow was captured.

Moroney et al. (2015) developed a multiscale model using an Representative Element Volume (REV) approach, where the bimodal size distribution of the coffee particles was represented using two mean characteristic diameters. Cameron et al. (2020) aimed to study variability of espresso extraction also using a continuous model that accounted for the soluble coffee diffusion process inside the porous particles. Further results were reported predicting the experimental total soluble solids content by applying a pore diffusion model on the internal particle pores using a weighted-average diffusion coefficient (Corrochano, 2017).

Recent studies have also described the extraction of individual espresso components. Beverly et al. (2020) proposed an experiment-validated model to predict the aroma extraction, indicating the importance of properties like polarity and partition coefficient on the diffusion-limited process step. Kuhn et al. (2017) formulated a mechanistic model to predict the concentration of the individual non-volatile components as function of time using semi-empirical lumped parameters.

Apart from espresso extraction, many other analogous studies have focused on packed bed reactor systems containing organic swelling granular material proposing modelling approaches for process optimization (Arora and Potůček, 2009; Reynolds et al., 2015; Alaqqad et al., 2012; Brodin et al., 2013; Potůček and Miklík, 2010). In all these studies a dispersion model has been employed to accurately describe the non-ideal flow in biomass packed beds.

In this work we aim to extend an existing espresso extraction model from Moroney et al. (2015) by accounting for the dispersive water flow through the coffee packed bed characterized by water residence time experiments. Additional equations were integrated in the model to determine the concentration of individual components in the extracting brew. The extraction of these components from the particle internal pores was set to be dependent on the overall extracting solids via the change in the particles porosity. Moreover, with the purpose of providing more detailed information about the early stages of the coffee extraction a completely dry coffee bed has been assumed, which subsequently gets wetted as water travels through it in the axial direction. This approach differs from other authors in the fact that no initial interparticle concentrations need to be assumed. Therefore, the influence of the particle wetting in the final extraction times can be more accurately described. Such a model could contribute to identifying the optimal extraction conditions from controllable parameters, such as particle size to improve the extraction efficiency, and the amount of coffee used per cup.

2. Materials and methods

2.1. Determination of water residence time distribution and dispersion coefficient

For the determination of the mean residence time inside the packed bed and the portafilter which is holding the coffee bed, the approach described by Danckwerts (1953) was followed. The residence time distribution (RTD) curve is defined in Equation (1) as follows:

$$E_i(t) = \frac{C_i}{\sum C_i \Delta t_i} \; with \; \sum_0^\infty E_i \Delta t_i = 1 \tag{1}$$

where C_i (kg/m^3) is the concentration of the tracer and Δt (s) the corresponding time step at instant i.. The tracer instant concentration was recorded at the exit of the portafilter. The corresponding mean residence time was defined as:

$$\bar{t} = \frac{\sum C_i t_i \Delta t_i}{\sum C_i \Delta t_i} \tag{2}$$

The tracer mean residence time was then compared with the theoretical mean residence time of a packed bed (Levenspiel, 1972) defined in Equation (3) as follows:

$$\tau = \frac{V_T}{Q} = \frac{\left(m_{coffee}/\rho_{bed}\right)\varepsilon_{bed}}{uA} \tag{3}$$

where V_T (m^3) is the reactor volume, in this case the portafilter, Q (m^3/s) is the volumetric flow rate, A (m^2) the cross-sectional area of the portafilter, u (m/s) the superficial flow velocity, m_{coffee} (kg) the coffee dosage, ρ_{bed} (kg/m^3) the bulk density of the bed, and ε_{bed} (−) the porosity of the bed.

The used dimensionless group to determine the extent of axial dispersion in the flow inside the packed bed was the Bodenstein number, defined as the ratio between convective and dispersive transport as follows:

$$Bo = \frac{vL}{D_{ax}} \tag{4}$$

where D_{ax} (m^2/s) represents the axial dispersion coefficient, v (m/s) the interstitial flow velocity and L (m) the bed length. With the Bodenstein number, a dimensionless time θ, a dimensionless concentration C and length X, the following dimensionless dispersion-convection equation is derived:

$$\frac{\partial C}{\partial \theta} = \frac{1}{Bo}\frac{\partial^2 C}{\partial X^2} - \frac{\partial C}{\partial X} \tag{5}$$

In the context of an espresso packed bed reactor, a closed-closed system was considered. The assumption is valid as the flow is practically undisturbed as it enters and leaves the portafilter boundaries, as shown in Fig. 1. Different from an open-open system, there is no analytical way to solve Equation (5) for a closed-closed system. Apart from employing a numerical solution for the equation, the Bo number can be calculated implicitly. As described in Levenspiel (1972), the Bo number has a discontinuity at X = 0, and X = 1, considering that no backflow occurs. Therefore, the spread measure of the RTD curve could be defined as

$$\sigma^2 = \frac{\sum t_i^2 C_i \Delta t_i}{\sum C_i \Delta t_i} - \bar{t}^2 \tag{6}$$

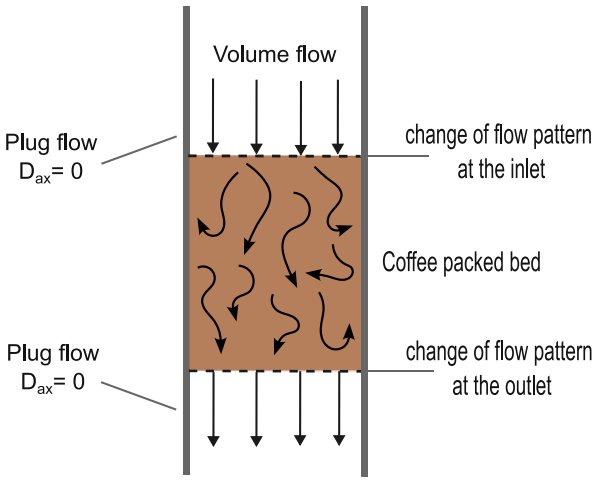

Fig. 1. Boundary conditions for the flow in a closed vessel. The volume flow pattern changes at the marked lines. The volume flow before and after the boundaries is unaltered and can be considered as plug flow with a axial diffusion coefficient close to zero.

where σ^2 (s^2) is the variance parameter that describes how much the system deviates from an ideal plug flow and approaches a full continuous stirred tank reactor (CSTR). Under this assumption, the Bodenstein *Bo* number can be then calculated implicitly with Equation (7) as follows:

$$\sigma_\alpha^2 = \frac{\sigma^2}{\bar{t}^2} = \frac{2}{Bo} - \frac{2}{Bo^2}\left(1 - e^{-Bo}\right) \quad (7)$$

2.2. Tracer pulse experiments set up

In order to measure the mean residence time of the water in the coffee packed bed, tracer pulse experiments, based on the method from Reynolds et al. (2015), were carried out using a KCl solution (0.01 g/ml and 134.14 mM) in an external parallel espresso extraction system (see Fig. 2) at 22 ± 2 °C water temperature, under the assumption that ambient water temperature would not cause any further internal modification of the bed, allowing the experiment to observe the current state of the bed. The tracer concentration was measured inline at the exit of the bed, as shown in Fig. 2, using a Conductivity Module 856 (Metrohm, Switzerland). The same piston pump model ULKA N15 (ULKA, Germany) as the Bezzera coffee machine (Vaca Guerra et al., 2023b) was used to ensure similar extraction conditions. A calibration curve was employed to correlate the measured conductivity with the concentration of the tracer.

Two groups of experiments were conducted: the first one where the coffee particle size distribution (PSD) was varied and a constant final cup mass of 30 g was brewed. In the second the mean residence time at different stages of the extraction was measured. For this second group, three experiments at constant PSD but different final brewed cups were performed: after 60 g of extracted brew (later stage), after 30 g (mid-range stage), and with the dry bed (initial stage).

In all experiments the extraction was firstly carried out in the Bezzera machine system at the same small portafilter and temperature initial conditions of 88 ± 2 °C as described in our previous work (Vaca Guerra et al., 2023a). The coffee dosage was adapted to ensure comparable volume flow conditions of average 3 ml/s in the parallel conductivity system as in our previously reported experiments (see Table 1). After the extraction, the portafilter was taken from the Bezzera machine and installed in the tracer pulse setup. The bed was then washed with 350 ml

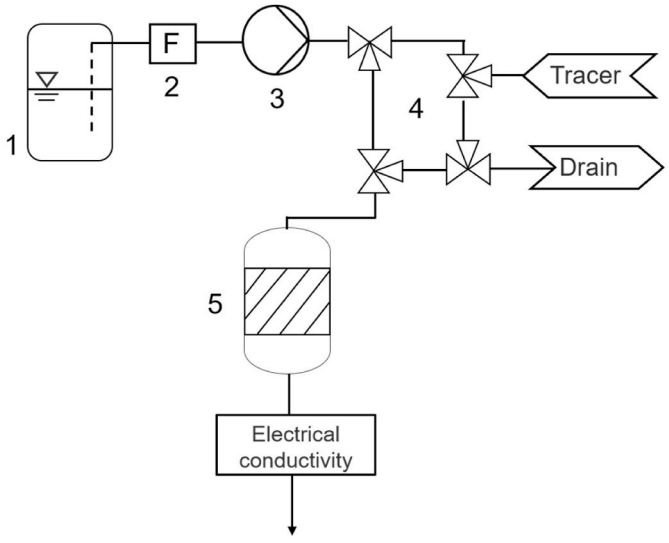

Fig. 2. Tracer pulse experiments set up diagram: Water container (1), flow meter (2), piston pump (3), tracer loop (4) with inlet and discharge, shower, water distributor and coffee bed (5), including portafilter and grid. The electrical conductivity was measured online at the bed exit. Experiments were performed with water at room temperature conditions (22–24 °C).

Table 1
Extraction conditions of the conducted tracer pulse experiments for the different PSDs. Average volume flow *Q* (ml/s), steady state interstitial velocity *v* (m/s), initial packed bed porosity ε_{bed}, and coffee dosage (g).

Parameter	Distribution A	Distribution B	Distribution C	Distribution D
Q (ml/s)	3.31 ± 0.17	3.11 ± 0.18	2.5 ± 0.17	2.64 ± 0.12
v (m/s)	4.96×10^{-3}	5.52×10^{-3}	4.12×10^{-3}	4.14×10^{-3}
ε_{bed} (−)	0.25	0.21	0.23	0.24
Dosage (g)	15.2	16.5	16.5	16.1

of demineralized water at 22 °C until a conductivity value < 0.15 ± 0.05 mS/cm^2 was reached. For the experiments, 9 ± 0.5 ml of KCl tracer were used to generate the tracer pulse. The tracer concentration took around 1 s to reach the packed bed due to the pipe volume.

2.3. Particle size distribution

Four particle size distributions were used in the extraction experiments as described in our previous work (Vaca Guerra et al., 2023a). A lower limit particle size Distribution A, a mid-range with distribution B, an upper-limit particle size with distribution C and a similar mid-range particle size with a larger size homogeneity on the coarse fraction with Distribution D. The cumulative volume-based distribution Q_3 (x) curves as well as the description of their mean diameters are shown in Fig. 3.

2.4. Total dissolved solids from experiments

The amount of soluble material in the coffee particles, defined as the total dissolved solids (TDS) was measured using a refractometer BS RMF340 (Bellingham and Stanley, England). A calibration curve to correlate the °Brix with the extracted dissolved solids was obtained using a gravimetric method where the brew was weighed before and after drying at 103 °C for 2 h based on ISO 11294-1994. The correlation TDS (g/g) = 0.085°Brix showed an R^2 = 0.98.

2.5. Extraction model

A Representative Element Volume (REV) method based on Moroney et al. (2015) for the espresso extraction modelling was adopted. Constant temperature during the whole extraction and across the length of the bed was assumed. The initial bed porosity ε_{bed} was considered to be homogenous throughout the bed and unaltered during the extraction. The model was developed in only the longitudinal direction, hence

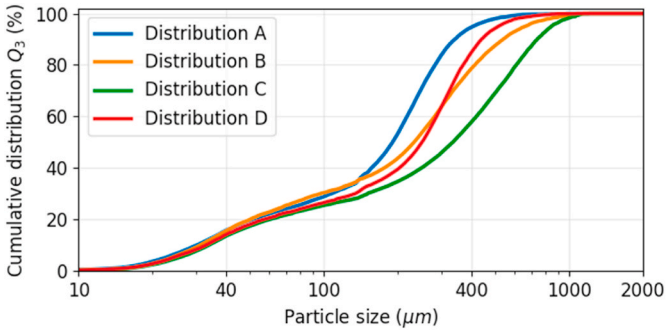

Fig. 3. Particle size distributions used in the extraction experiments reported in Vaca et al. (Vaca Guerra et al., 2023a). The lower size limit, distribution A with a value of $d_{3,2}$ = 105 μm, coarse fraction $d_{3,2}$ (dp > 100 μm) = 272 μm and $d_{4,3}$ = 325 μm; the middle range size limit, distribution B with a value of $d_{3,2}$ = 113 μm, coarse fraction $d_{3,2}$ (dp > 100 μm) = 343 μm and $d_{4,3}$ = 459 μm; and the upper size limit, distribution limit C with $d_{3,2}$ = 134 μm coarse fraction $d_{3,2}$ (dp > 100 μm) = 438 μm and, $d_{4,3}$ = 611 μm and the additional increase size uniformity distribution D with $d_{3,2}$ = 120 μm and coarse fraction $d_{3,2}$ (dp > 100 μm) = 337 μm.

radial diffusion was neglected and the bed length was assumed to remain constant during the whole extraction. A schematic representation of the extraction coffee model is found in Fig. 4. As it can be seen in the Figure, two main groups of particle sizes were assumed: a coarse volume fraction and the fine volume fraction where limiting cutoff particle size was 100 μm.

Transport through the internal pores of the particles: Diffusive mass transfer takes place from the inside of the particle kernels through the internal pore space to the bulk of flowing water around the particles. As the internal pores structure has a direct influence on the length of the diffusive path, the correlation of this parameter with the tortuosity proposed by Moroney et al. (2015) was incorporated in the lumped mass transfer coefficient α (m/s), defined in Equation (8) as:

$$\alpha = \alpha^* \frac{D_v}{l} (\varepsilon_{part})^{4/3} \tag{8}$$

where α* (−) is the lumped fitted parameter, D_v (m^2/s) the diffusion coefficient of the soluble component in water (in this case considered to be from caffeine in water), ε_{part} (−) is the particles porosity, l (m) is the average mean length of the coffee particles, in this work defined as half of the coarse fraction mean $d_{4,3}$ diameter. Accordingly, the total mass transport in the grains is defined in Equation (9) as follows:

$$\boldsymbol{A} = \alpha\, S_1 (C_v - C_h) \tag{9}$$

where C_v and C_h (kg/m^3) refer to the intragranular and intergranular averaged concentration respectively. The difference between C_v and C_h is accounting for the driving force of the diffusive mass transfer. The specific surface area parameter is defined as $S_1 = 6/d_{3,2coarse}$ with the Sauter mean diameter of the particles coarse volume fraction, with the assumption that only a fraction of particles is large enough to have pores ($d_p > 100$ μm).

Transport from the surface of the particles to the intergranular pores: The solubilization process taking place at the solid surface of the particles involves several complex phenomena. Therefore, it was assumed that all the soluble mass, present on the surface (represented as the volume fraction φ_{s0}) is already solubilized in an infinitesimal distance next to the solid surface. This solution has already reached the equilibrium; therefore, the concentration was considered to be the saturation concentration C_{sat}. The occurring mass transfer was then considered as an interphase mass transfer process, where the component molecules diffuse to the bulk flow as described in Equation (10):

$$\boldsymbol{B} = \beta\, S_2 (C_{sat} - C_h) \varphi_{c0} \psi_s \tag{10}$$

Here, the driving force for mass transfer is the concentration difference between the saturation concentration C_{sat} (kg/m^3) and the local interparticulate average concentration C_h (kg/m^3). φ_{c0} (−) is the total volume fraction of soluble coffee in the grains. The term ψ_s (−) is the remaining fraction of soluble coffee with respect to its initial volume fraction contained in the grains. This term serves as a limit factor in the whole extraction process as defined by Moroney et al. (2015). These parameters contained in the equation are determined experimentally. The specific surface area parameters are defined as $S_2 = 6/d_{3,2\ fines}$, with the Sauter mean diameter of the whole particle size distribution, which is dominated by the fines fraction. The lumped mass transfer coefficient β (m/s) is defined in Equation (11) as:

$$\beta = \beta^* \frac{2D_v}{m} \tag{11}$$

where β* (−) is the lumped fitted parameter, m (m) is the mean diameter of the particles open pores proven to be approximately 40 μm (Schenker et al., 2000). Note that the same diffusion coefficient D_v was used as in Equation (8) for α. After defining the two main mass transfer equations, the whole extraction process could be modeled by solving Equation (12)–(15) simultaneously:

$$\varepsilon_{bed} \frac{\partial C_h}{\partial t} = \frac{\partial}{\partial z} \left(D_{ax} \frac{\partial C_h}{\partial z} - u C_h \right) + (1 - \varepsilon_{bed})(\boldsymbol{A} + \boldsymbol{B}) \tag{12}$$

$$\frac{\partial \varepsilon_{part} C_v}{\partial t} = -\boldsymbol{A} \tag{13}$$

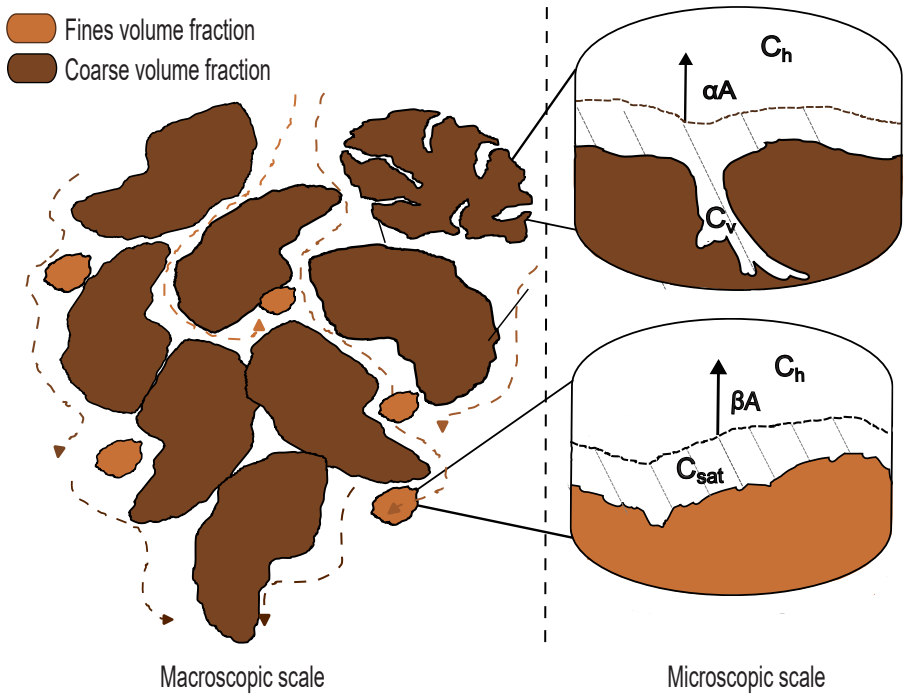

Fig. 4. Representation of the coffee extraction model based on Moroney et al., (2015). The mass transfer coefficient β corresponds to the fines volume fraction ($d_p <$ 100 μm) and mass transfer coefficient α to the coarse volume fraction ($d_p > 100$ μm). C_h (kg/m^3) is the intergranular concentration at the bulk water, C_{sat} (kg/m^3) saturation concentration at the particles surfaces, C_v (kg/m^3) concentration at the particle internal pores and A (m^2) the surface area where extraction takes place.

$$\frac{\partial \varepsilon_{part}}{\partial t} = -\frac{1}{r_s}\frac{\partial \psi_s}{\partial t} \tag{14}$$

$$\frac{\partial \psi_s}{\partial t} = -\boldsymbol{B}\frac{r_s}{C_s} \tag{15}$$

where ε_{bed} (−) is the initial packed bed porosity, u (m/s) is the superficial velocity, r_s (−) the inverse of the initial soluble coffee volume fraction at the coarse and fines particles surface φ_{s0} and C_s (kg/m^3) is the density of the coffee solid matrix, determined to be 1304 kg/m^3 in our previous work (Vaca Guerra et al., 2023b). The parameters **A** and **B** are expressed as source/sink terms.

2.6. Modelling extraction of individual species

For predicting the instant extracted concentration of individual species in espresso, the proposed model was extended by including additional equations to describe the mass transport of the specific components from the particle surfaces and internal pores to the intergranular pores. It was assumed based on the low concentrations and physicochemical properties, such as polarity and molecular weight, of the components studied (caffeine, trigonelline and 5-CQA), that interactions between components are negligible. Besides, in other relevant works (Kuhn et al., 2017; Schmieder et al., 2023) which have studied the extraction of the same components, also have not reported major interactions. Furthermore, molecular interactions induced by other components in the coffee extract are not considered in this work. With these assumptions the prediction of extraction kinetics of every component can be carried out independently. This leads to the following system of equations:

$$\varepsilon_{bed}\frac{\partial c_{hi}}{\partial t} = \frac{\partial}{\partial z}\left(D_{ax}\frac{\partial c_{hi}}{\partial z} - uc_{hi}\right) + (1-\varepsilon_{bed})(\boldsymbol{A}+\boldsymbol{B}) \tag{16}$$

$$\frac{\partial c_{vi}}{\partial t} = \frac{-\boldsymbol{A} - \left(\frac{\partial \varepsilon_{part}}{\partial t}\right)c_{vi}}{\varepsilon_{part}} \tag{17}$$

$$\frac{\partial \psi_i}{\partial t} = -\boldsymbol{B}\frac{r_i}{C_s} \tag{18}$$

where c_{hi} (kg/m^3) is the intergranular concentration of component i, c_{vi} (kg/m^3) the concentration of component i within the internal pores of the particles, r_i (−) the inverse of the initial volume fraction of the respective component at the coarse and fines particles surface φ_{s0}, and ψ_i the remaining volume fraction of component i, both defined at the particle surface. The value of the particles porosity as a function of time and bed length is obtained from solving the total dissolved solids system of equations. Hence, the individual species extraction directly depends on the performance of the overall extraction.

2.7. Initial bed filling phase and dispersed volume flow

Existing espresso extraction models from published works assume an already water-filled bed as initial condition (Cameron et al., 2020; Moroney et al., 2015). Accordingly, experimental results and linear correlations were necessary to provide initial concentration conditions along the bed. However, important information regarding how much soluble material is extracted in the end, happens during the initial water filling phase. The flow regime during this initial phase highly depends on the packed bed conditions, like packed bed porosity, particle size distribution and temperature. In this work we propose an approach to include the filling phase into the extraction model. To do this, additional parameters were integrated into the system of equations described previously. The packed bed is considered to be dry at t = 0, and the water front is modeled as an activation step, with the same dispersed flow pattern as the rest of the extracting water flow. Equation (16) describes this activation step as follows (Reynolds, 2019):

$$\varepsilon_{bed}\frac{\partial Y_{step}}{\partial t} = \frac{\partial}{\partial z}\left(D_{ax}\frac{\partial Y_{step}}{\partial z} - uY_{step}\right) \tag{19}$$

where u (m/s) is the superficial velocity and Y_{step} (−) is a fictitious parameter to represent the water front in the packed bed filling phase. Supposing Y_{step} has a concentration of 1 kg/kg it has the same flow dispersion as the extracting water. By solving this additional equation, the parameter Y_{step} serves as a switch for the rest of the equations, hence it goes from 0 to 1, and was added as a multiplication factor for Equations (12) and (13),15, 16, 17 and 18.

The system of partial differential equations was discretized using an upwind scheme. The number of discretization elements or cells was chosen as 20, taking care that the step was not smaller than the coffee particles. Thus, the cell or step size was 7.05×10^{-4} m. It was confirmed that the solution was independent of the step size in a range of 10–20 steps. . A Runge-Kutta numerical solution for the system of the discretized equations was used and was embedded in the MATLAB function ode53s with an adaptive time step.

3. Results and discussion

3.1. Analysis of the residence time distribution curve results

As previously described, the mean residence time of the water in the packed bed was investigated by means of tracer pulse experiments using different particle size distributions. Despite the fact that the tracer measurements were carried out in a parallel set up shown in Fig. 2, the volume flow rate with an average value of 3.1 ± 0.31 ml/s was similar to the one reported in our previous work. Therefore, it can be assumed that the extractions occurred under comparable conditions. The packed bed was considered to have a constant length value of 13.4 mm and a diameter of 59 mm. The obtained instant conductivities from the tracer pulse experiments were translated into concentration values using a calibration curve. Equation (1) was then used to calculate the residence time distribution curve. Fig. 5 shows the results of first groups of experiments using four different PSDs after 30 g of brew coffee. For the second group of experiments at constant PSD, distribution B was selected for its mean diameter characteristics. Different from distributions A and C, that represent the extremes of technically feasible particle size range, distribution B represents the middle range of particle sizes,

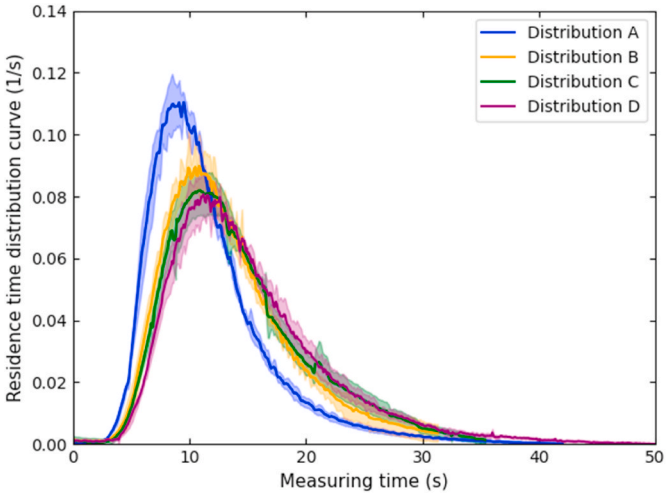

Fig. 5. Average residence time distribution curve (1/s) as function of the measuring time (s) obtained from the tracer pulse experiments using Distribution A, B, C and D. All experiments were carried out in triplicate. The error shades correspond to the standard deviation from the triplicate experiment repetitions.

being therefore of larger interest for espresso extraction applications. However, any relevant distribution can be used in the future using the proposed framework in this study. Fig. 6 contains the results of experiments using a constant PSD (Distribution B), at different extraction stages. Tracer mean residence times were calculated with the help of Equation (2). The obtained values are shown in Table 2 and Table 3 for the two groups of experiments, respectively. Results indicate that the tracer mean residence time is larger than the value of τ (s), the mean residence time calculated with Equation (3) for all experiments. The water flow path inside the bed may then be highly tortuous, leading to larger residence times. After 30g of brewed coffee the mean residence time is on average larger by a mean factor value of 5.09 ± 0.53. The highest value was found using the midrange distribution B with a factor of 6, and the lowest with the larger limit distribution C with a value of 4.7 (see Table 2). Due to the small deviations between the measured residence time factors, it is assumed that this parameter is independent of the particle size distribution at similar volume flow conditions.

When comparing the results from different stages of extraction at constant PSD, the calculated tracer mean residence time average was around 4.89 times larger than the calculated average of the mean residence time τ (s), with an increasing trend as the extraction progressed (see Table 3). This could be due to the further consolidation of the bed observed and quantified by other authors (Corrochano et al., 2015).

Note that these mean residence time values do not take into account possible changes in the bed porosity; they were determined using the initial dry bed porosity; thus, the actual mean residence time values may be relatively higher (if the particles porosity values are expected to increase due to extracted coffee mass). However, additional information of the real bed porosity may be required to estimate it accurately.

It is unlikely that the delay in the mean residence time distribution curves could be caused by a strong interaction of the tracer with the solid matrix, such as solute adsorption onto the coffee particles, as considered by other authors (Reynolds et al., 2015). Severe absorption of the tracer would rather cause a very long and flat tailing in the residence time distribution which is not to be found in the presented results.

3.2. Comparison of the axial flow dispersion using different particle size distributions

The dispersion in the volume flow inside the packed bed was

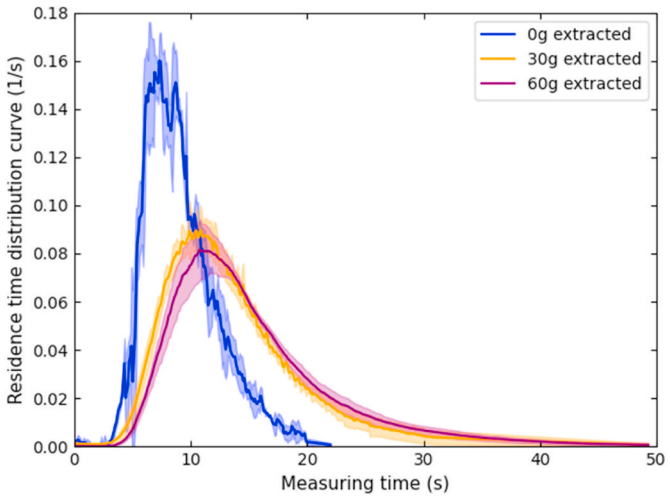

Fig. 6. Average residence time distribution (1/s) as function of the measuring time (s) obtained from the tracer pulse experiments using Distribution B as a constant PSD at different stages of extraction: Initial stage with 0g of extracted brew (blue), Mid-stage after 30g of extracted brew (orange), late stage after 60g of extracted brew (purple). The error shades correspond to the standard deviation from the triplicate experiment repetitions.

Table 2
Average volume flow Q (ml/s) conditions for experiments using distribution A, B, C and D and the obtained mean residence time τ (s) from Equation (3), tracer mean residence time $\bar{t}$ (s) calculated from Equation (2), and the Bodenstein number Bo (−) solved from Equation (7). The extraction was performed up to 30g of extracted brew.

Distribution	Q (ml/s)	τ (s)	$\bar{t}$ (s)	Bo (−)
A	3.31 ± 0.17	2.47 ± 0.39	11.75 ± 0.39	8.70 ± 0.84
B	3.11 ± 0.18	2.28 ± 0.27	13.68 ± 0.84	10.01 ± 2.82
C	2.50 ± 0.17	3.02 ± 0.37	14.3 ± 0.71	10.36 ± 1.15
D	2.64 ± 0.12	3.14 ± 0.25	15.1 ± 0.38	8.98 ± 1.07

Table 3
Average volume flow Q (ml/s) conditions for experiments using constant PSD Distribution B at the initial extraction stage (0g of extracted brew), mid-stage extraction, after 30g of extracted brew and the late stage extraction after 60g of extracted brew. Additionally, the obtained mean residence time τ (s), tracer mean residence time $\bar{t}$ (s) and the Bodenstein number Bo (−).

Extraction state	Q (ml/s)	τ (s)	$\bar{t}$ (s)	Bo (−)
0 (initial state)	3.76 ± 0.19	1.81 ± 0.11	9.18 ± 0.35	16.84 ± 0.47
After 30g	3.11 ± 0.18	2.28 ± 0.27	13.68 ± 0.84	10.01 ± 2.82
After 60g	3.17 ± 0.15	2.44 ± 0.12	15.56 ± 1.35	7.74 ± 1.29

characterized using the Bodenstein number (Bo) defined in Equation (4). This number was solved from Equation (7), after calculating the σ^2 from Equation (6). The results for the two groups of experiments are also presented in Tables 2 and 3. The obtained reciprocal value of the Bo number was larger than 0.01 in all experiments, which indicates a dispersive flow; hence plug flow should not be assumed according to Levenspiel (1972). The values shown in Table 2 indicate that in the investigated range, the Bo number is independent of the particle size at similar extraction volume flow conditions. However, the Bo number was found to decrease as a function of the extracted brew, hence the stage of the extraction. As the extraction proceeds Bo number was found to be 16.84 for the dry bed, then 10.01 at the middle extraction stage after 30 g of extracted brew, and finally changing only slightly after 60 g of extracted brew with a value of 7.74. This indicates the highly dynamic processes occurring inside the bed which impacts the flow velocity profile of the water along the extraction. Apparently, the bed starts at a condition that is closer to a plug flow regime with relatively low axial dispersion (larger Bo numbers). Then, the axial diffusion increases probably due to particle swelling, erosion, fines migration and bed consolidation reaching a final constant value at steady state, as studied and characterized by our group and other authors. All these effects may contribute to the modification of the dispersed flow velocity through the bed.

Moreover, additional experiments should be carried out to establish the correlation between the longitudinal flow diffusion and the actual interstitial velocity as function of the bed porosity.

3.3. Fitting model parameters to experiment instant concentrations at bed exit

The previous experiment results have shown that the dispersive flow remains relatively constant for the whole extraction, with exception of the initial filling phase, where the dispersion number was found to be relatively smaller (see Table 3). In order to represent this highly dynamic behavior, Equation (20) was defined to describe the transition between the different axial diffusion coefficient regimes during the extraction, in line with our experimental observations:

$$D_{ax} = \left(1 - Y_{step}\right) D_{ax0} + Y_{step} D_{axss} \tag{20}$$

where D_{ax} is the effective axial dispersion coefficient at certain time of the transition of the filling phase, D_{ax0} is the initial axial dispersion

coefficient, determined from the dry bed experiments and D_{axss} is the steady-state axial dispersion coefficient; both obtained from the *Bo* number shown in Tables 2 and 3. For the value of D_{axss} an average Bo number value of 9.76 ± 1.86 was used, whereas for D_{ax0} was the initial stage Bo number of 16.84 ± 0.47 from distribution B experiments (under the assumption that this Bo number at the initial stage is also conserved for all PSDs in this work). When the coffee bed is completely filled, Y_{step} will have a value of 1 along the bed, hence the effective axial dispersion coefficient will reach the value of D_{axss}.

To fit the parameters of the model proposed in this work, experiments presented in our previous publication on the progressive extraction of several marker compounds (among them caffeine, trigonelline and chlorogenic acid 5-CQA) (Vaca Guerra et al., 2023a) were used. The assumption was made that the mass of total dissolved solids (TDS) and of every particular component are homogenously distributed in the whole grain volume (Moroney et al., 2015). The volume flow velocity was taken from the steady-state conditions of the above-mentioned experiments, and since the evolution of the bed porosity was not determined in this work, it was assumed that both parameters to remain constant during the whole extraction. The maximum extracted mass was determined in the experiments using the finest PSD A. This is also the reason why the experiment results from this distribution were used for fitting the model parameters. The parameters φ_{c0}, φ_{s0} were calculated considering that only a volume fraction of particles (<100 μm) are large enough to contain pores with an average size of 40 μm. This volume fraction (%) depends on the particle size distribution used (see Fig. 3).

A summary of the experimental conditions relevant for describing espresso extraction, such as particle size characteristics, initial packed bed porosity ε_{bed}, and interstitial flow velocity v is given in Table 4. The initial value of the particle porosity ε_{part} was assumed to be 0.47, based on mercury porosimetry results obtained for the same coffee grain batch (Vaca Guerra et al., 2023b). Table 5 shows the initial conditions applied for model fitting to the extraction experiments from distribution A.

In summary, the initial conditions applied for solving Equations (12)–(15) are:

$$C_h(z,0) = 0$$
$$C_v(z,0) = C_{v0}$$
$$\varepsilon_{part}(z,0) = \varepsilon_{0part}$$
$$\psi_s(z,0) = 1$$
$$Y_{step}(z,0) = 0$$

together with the boundary conditions:

$$C_h(L,0) = 0$$
$$P(0,t) = 0$$
$$P(L,t) = \Delta P$$
$$Y_{step}(0,t) = 1$$

These boundary and initial conditions reflect the assumption that the bed is dry at the considered t = 0. The variable *P* (bar) refers to the pressure drop across the bed, and was not included in the equations so far because the interstitial velocity was taken directly from the experimental data (see Table 4). However, it is necessary here to establish the direction of the flow. Nonetheless, note that the volume flow could be determined with an independent correlation, for instance, the one proposed in our previous work (Vaca Guerra et al., 2023a, Vaca Guerra et al., 2023b).

The α* and β* and the saturation concentrations C_{sat} of the TDS and the three components were fitting parameters of the proposed model. C_{sat} was then assumed to be the maximum concentration attainable at the given experimental conditions. These values may be specific for the temperature and pressure conditions, as well as coffee type and roasting used.

The fitting was made between the values from the last layer of the discretization, specifically at the exit of the bed, and the experimental data using the fminsearch function in Matlab, where the difference between the squared errors was minimized. The relative tolerance was set at a value of 1×10^{-8} and the absolute tolerance of 1×10^{-10}. The initial guess values for the algorithm to fit the TDS experiments were 0.1 for both α* and β*. The initial C_{sat} was set to be internal pores concentration Cv_0. The lower limit for C_{sat} was also set to be Cv_0. For the individual components, the initial conditions for α* and β* were taken from the fitted parameters of the TDS.

The model fitting results for the instant concentration at bed exit for

Table 4
Extraction conditions of the conducted experiments from the previous work (Vaca Guerra et al.). *Q* (ml/s) refers to the average volume flow, *v* (m/s) to the interstitial velocity, initial packed bed porosity ε_{bed} (−), $d_{3,2fines}$ (μm) the Sauter mean diameter of distribution fines fraction (<100 μm), $d_{3,2coarse}$ (μm) the Sauter mean diameter of the coarse fraction (>100 μm), *l* (m) is the half of the mean $d_{4,3}$ diameter of the respective distribution coarse fraction.

Parameter	Distribution A	Distribution B	Distribution C
Q (ml/s)	3.43 ± 0.07	3.98 ± 0.4	3.61 ± 0.3
v (m/s)	4.9×10^{-3}	5.6×10^{-3}	5.9×10^{-3}
ε_{bed} (−)	0.26	0.25	0.22
$d_{3,2fines}$ (μm)	105	113	134
$d_{3,2coarse}$ (μm)	272	343	348
Dosage (g)	17.1	17.25	18.23
l (μm)	163	230	306

Table 5
Modeling initial conditions for experiments using distribution A, φ_{C0} (−) refers to the initial TDS or respective component volume fraction, φ_{s0} (−) initial TDS or component volume fraction present in the coarse and fines particles surface, rs (−) the respective inverse value, C_{v0} (kg/m^3) the initial TDS or respective component concentration in the particles pores.

Distribution A	TDS	Caffeine	Trigonelline	5-CQA
φ_{C0} (−)	0.16	0.007	0.0027	0.0042
φ_{s0} (−)	0.047	0.002	0.0007	0.0011
r_s (−)	22.2	485	1278.7	833
C_{v0} (kg/m^3)	513	22.2	8.26	13.46

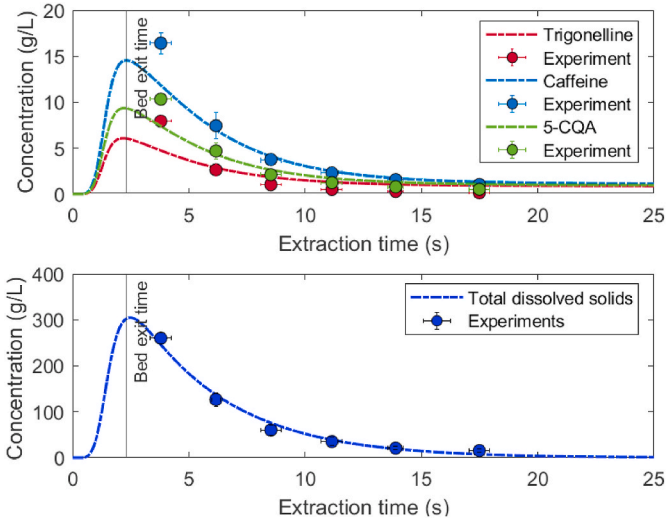

Fig. 7. Instant concentration at bed exit (g/L) as a function of extraction time (s) from experiments using the lower particle size limit distribution A. The graph points account for the experiments measured concentration, whereas the dotted lines refer to results from the model for the individual components, trigonelline (red), caffeine (blue), 5-CQA (green), and total dissolved solids. The error bars at the points correspond to the standard deviation from the triplicate experiment repetitions. Bed exit time was determined with the mean residence time from Equation (3).

extraction experiments using distribution A are presented in Fig. 7. The obtained values of the fitted parameters are presented in Table 6 from where it can be seen that trigonelline had the largest fitted saturation concentration with a value of 74.86 kg/m^3, while caffeine the lowest with 54.53 kg/m^3. A large correspondence with the TDS experimental data was obtained with the model, with a coefficient of determination of $R^2 = 0.99$ (see Figure in Appendix). Moreover, the fitting of the individual components was less accurate, with an average value of $R^2 = 0.83$ (see Figure in Appendix). This could be attributed to a non-homogenous distribution of the components in the grains, hence higher concentrations of these components are present in the exposed kernels, which are abundant in this particular distribution, leading to a rapid increase in the concentration at the initial extraction stage.

Further analysis of the complete system of results of distribution A experiments including also concentrations at the particle pores, particle porosity and other variables is included in the Appendix.

The bed exit time in Fig. 7 refers to the extraction time point at which the brew starts flowing out of the bed, thus the bed filling process is completed. This parameter was determined using the mean residence time in Equation (3). However, due to the axial dispersed flow the value could only be considered as an approximation. The bed exit time is essential for determining the final cup concentration. A step-by-step procedure applied to determine the final cup concentrations at any extraction time from the model predictions can also be found in the Appendix.

3.4. Model validation with experiments using different particle size distributions

To validate the model, the obtained values of α*, β* and C_{sat} (see Table 6) were used to predict the extraction from experiments using two other particle size distributions. Given the assumptions that the total available mass of soluble coffee (determined in the experiments with distribution A) is an intrinsic property of the grains, and that the particle porosity is homogeneous along all particles, the same C_{v0} values were used. Table 7 shows the modelling parameters φ_{C0} and φ_{s0}.

Results are shown in Fig. 8 for distribution B, and Fig. 9 for distribution C. The predicted instant concentration at the bed exit shows a good agreement with the TDS experiment values for distribution B and distribution C with $R^2 = 0.95$ and $R^2 = 0.97$ respectively (see Figure in Appendix). The predicted concentrations for the individual components was relatively better than for distribution A, with an average $R^2 = 0.90$ for distribution B and $R^2 = 0.95$ for distribution C.

These results may be specific to the extraction conditions applied in our experiments, thus the model should be further tested against experiments outside of the range of the previously studied flow pressure conditions. The obtained parameters of mass transfer and axial diffusion coefficients as well as the saturation concentrations, may be dependent on the volume flow rate, extraction temperature and length of the bed and coffee grains type and roasting.

3.5. Analysis of calculated mass transfer coefficients from individual components

As expected, the calculated parameter β (see Equation (11)), which is the mass transfer coefficient related to extraction from the surface of the particles was found to be larger than α (see Equation (8)) in all cases because of the extraction hindrance inside the particle pores, which means the diffusive tortuosity path involved for the mass transfer from the inside the pores is longer than for the convection path (Spiro and Selwood, 1984).

Fig. 10 shows the decreasing values of α inversely proportional to the mean particle size from the different PSD experiments. The mass transfer α from the individual components were found to be relatively larger than the obtained parameters of the TDS, as shown in Fig. 10. This means that the three components are extracted relatively faster than the average overall soluble solids. The mass transfer α of the TDS could then be understood as the result of a mass weighted average of all soluble components, as proposed by some other authors (Corrochano, 2017). It makes therefore sense that the obtained mass transfer coefficients for caffeine, which is considerably more abundant component in the overall TDS, is closer to the overall TDS value, whereas trigonelline, and 5-CQA with larger fitted values are considerably less abundant in extracted brew (see values of φ_{C0} in Table 5).

The mass transfer coefficient β was conserved for the different PSD experiments, as the average diameter of the pores, where the mass transfer takes place, was assumed to be constant and intrinsic of the coffee particles. Moreover, the results of β show a similar trend as α, as it can be seen in Fig. 11. The obtained values for the components were relatively larger than the TDS, being also trigonelline the component with the highest value.

Table 6
Obtained fitting parameters for experiments with Distribution A. C_{sat} (kg/m^3) refers to the fitted saturation concentration of the total dissolved solids and respective individual components, α* (−) and β* (−) the fitted mass transfer coefficients.

Distribution A	TDS	Caffeine	Trigonelline	5-CQA
C_{sat} (kg/m^3)	513	54.53	74.86	65.86
α* (−)	3.4	7.33	9.27	8.72
β* (−)	0.29	1.21	1.8	1.5

Table 7
Modeling initial conditions for experiments using distribution B and distribution C. φ_{C0} (−) refers to the initial TDS or respective component volume fraction, φ_{s0} (−) initial TDS or component volume fraction present in the coarse and fines particles surface, rs (−) the respective inverse value.

Distribution B	TDS	Caffeine	Trigonelline	5-CQA
φ_{s0} (−)	0.048	0.0021	0.0008	0.001
r_s (−)	21	459	1209	788
Distribution C				
φ_{s0} (−)	0.039	0.0018	0.0007	0.001
r_s (−)	25	548	1445	941

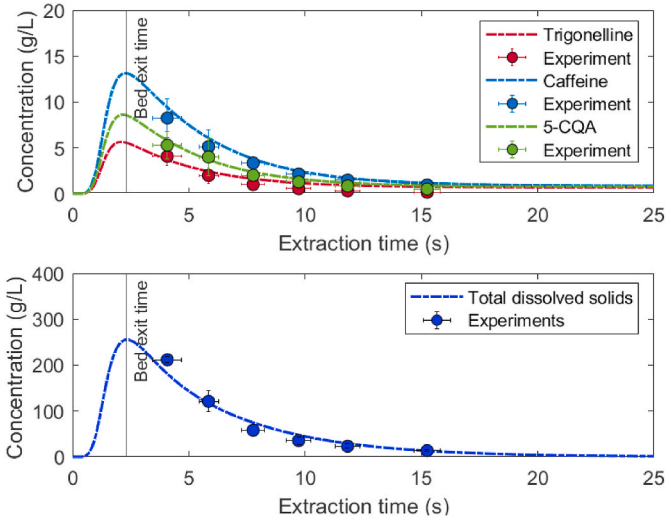

Fig. 8. Instant concentration at bed exit (g/L) as a function of extraction time (s) from experiments using the mid-range particle size distribution B. The graph points account for the experiments measured concentration, whereas the dotted lines refer to results from the model for the individual components, trigonelline (red), caffeine (blue), 5-CQA (green), and total dissolved solids. The error bars at the points correspond to the standard deviation from the triplicate experiment repetitions. Bed exit time was determined with the mean residence time from Equation (3).

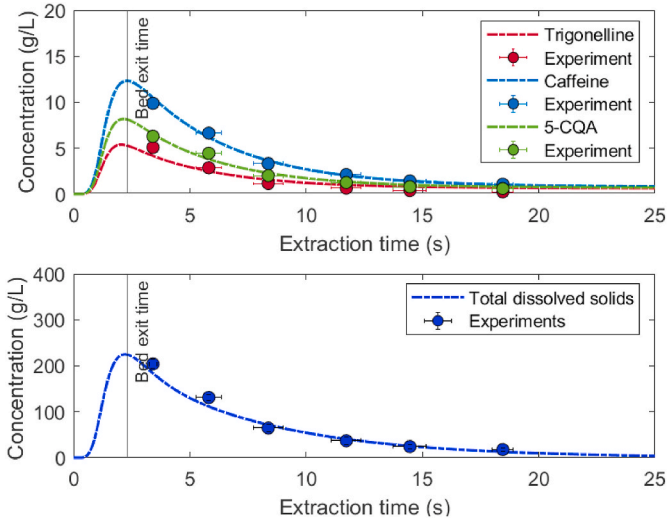

Fig. 9. Instant concentration at bed exit (g/L) as a function of extraction time (s) from experiments using the upper particle size limit distribution C. The graph points account for the experiments measured concentration, whereas the dotted lines refer to results from the model for the individual components, trigonelline (red), caffeine (blue), 5-CQA (green), and total dissolved solids. The error bars at the points correspond to the standard deviation from the triplicate experiment repetitions. Bed exit time was determined with the mean residence time from Equation (3).

Standard deviation between the fitted values of β among the three components was found to be 3.26 × 10^{-5} m/s, therefore, relatively larger than the standard deviation between α values with a value of 1.35 × 10^{-5} m/s. Accordingly, a more homogenous extraction, from a component concentration point of view, would be expected when mass transfer α from the inside the particles pores dominate over β. On the other hand, a more selective extraction may be then achieved when the extraction from the particles surface is promoted by increasing the particles specific surface area. This selectivity may be directly dependent on the components individual properties.

As mentioned before, the value of α increases as the particle size is reduced, approaching closer to the value of parameter β. It is possible

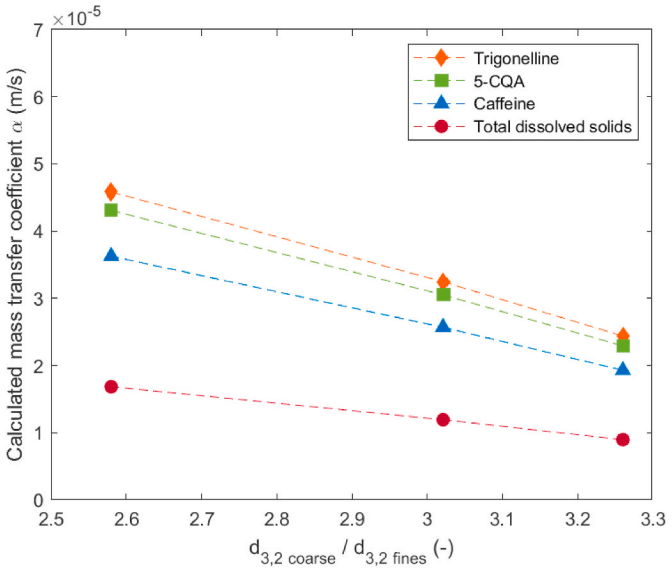

Fig. 10. Obtained mass transfer coefficient α (m/s) using the initial $\varepsilon_{part} = 0.47$ for the analysis as function of the particle size ratio $d_{3,2coarse}/d_{3,2\ fines}$ (−) from the total dissolved solids TDS and the individual components trigonelline, 5-CQA and caffeine. The dotted lines are only for a better data visualization.

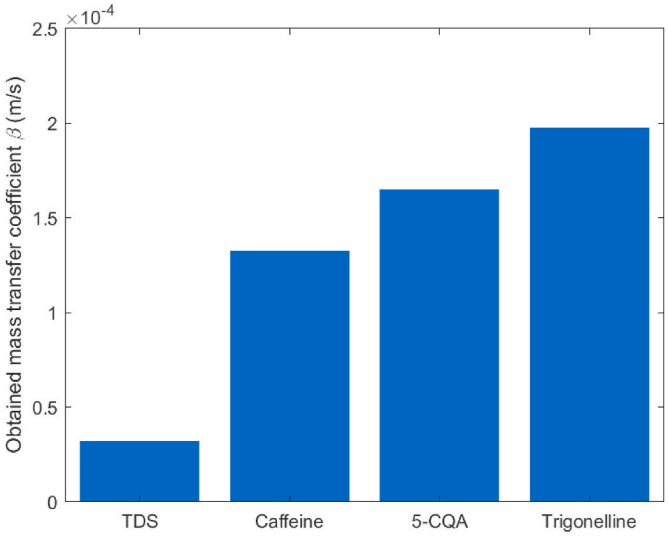

Fig. 11. Comparison of the obtained mass transfer coefficient β (m/s) related to the extraction from the surface of the particles, for the total dissolved solids, caffeine, 5-CQA and Trigonelline.

that in this case, the internal cell structures are completely torn apart and exposed to the water flow, reducing the intraparticle diffusion path. Moreover, to make a more physically accurate comparison between the two parameters α and β, we suggest including a partition coefficient in the model to account for the interaction between the solid matrix and the liquid layer next to it, as the one proposed by Corrochano (2017).

The components calculated mass transfer values α and β were therefore correlated with their respective polarities reported in the National Center of Biotechnology Information (National Center for Biotechnology Information, 2022). An exponential equation was used to correlate the calculated values from the three studied components with their respective polarities. Fig. 12 shows the fitting results of mass transfer coefficient α with a coefficient of determination $R^2 = 0.62$, and for β with a $R^2 = 0.84$ respectively. Despite the fact that the sample size in the reported results is not extensive enough to deliver any conclusions, it does show a trend. Relatively larger mass transfer coefficients α,

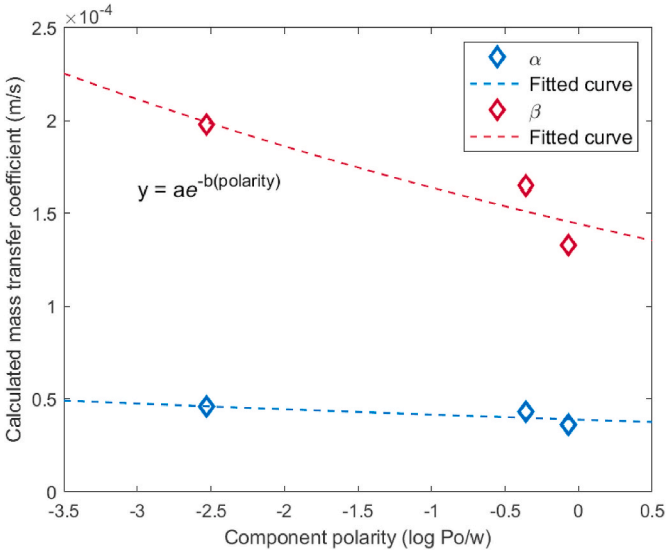

Fig. 12. Exponential correlation between the obtained mass transfer coefficient α (from distribution A) and β for trigonelline, 5-CQA and caffeine with their respective polarities. The obtained R^2 for the fitted equation are 0.62 for mass transfer coefficient α and 0.83 for β. The fitted parameters are found in Table 9 in the Appendix.

and β were found for the more polar components, in this case trigonelline. These results are in accordance to our previous work (Vaca Guerra et al., 2023b). Moreover, results also show that β, the coefficient related to the mass transfer from the surfaces, may have a more extensive dependence on the components polarity; hence a better correlation with this parameter was obtained. On the other hand, α which is related to the mass transfer from the inside the pores, may be largely impacted by other factors as well, such as components interactions or molecular diffusivities. To improve this correlation, experiment data with a larger number of studied components would be needed. The obtained equation could be then used to estimate the extraction kinetics from any individual component based only on their properties like polarity.

3.6. Importance of considering axial dispersion in espresso extraction modeling

In this section a quantitative comparison of varying the axial dispersion in the proposed espresso extraction model is presented. Using the same extraction conditions from the previous sections, together with the obtained fitted parameters for α*, β*, and the $C_{sat,}$ the effective axial dispersion coefficients from the initial filling phase D_{ax0} and steady state D_{axss} phase were varied with the same proportion for four different cases. Fig. 13 shows the analysis results from the four cases for the TDS extraction using distribution A. Case 3 refers to the results presented previously, using the values from Tables 4 and 5. The axial dispersion coefficients were obtained from Equation (4) and the averaged *Bo* numbers from tracer pulse experiments (see Tables 2 and 3). The axial coefficients from case 2 and case 4 correspond to a 50% decrease and increment of the obtained D_{ax0} and D_{axss} values, respectively. In case 1, the axial dispersion was completely neglected. From the Figure is clear that the initial filling activation step, defined in Equation (19) (also highly dependent on the diffusion), works as an accurate approximation of the initial intergranular concentration (which was alternatively assumed from experiments by Moroney et al. (2015)). However, the parameters α* and β* are limited to the specific flow conditions used in this study. The comparison clearly shows that diminishing the axial dispersion leads to an overestimation of the instant extracted TDS concentration and vice versa. Therefore, for different flow velocity conditions, experiments where the axial diffusion was also characterized, would be then necessary to obtain mass transfer coefficients that accurate predict the extraction. These could be then compared to each other to study the impact of volume flow in espresso extraction.

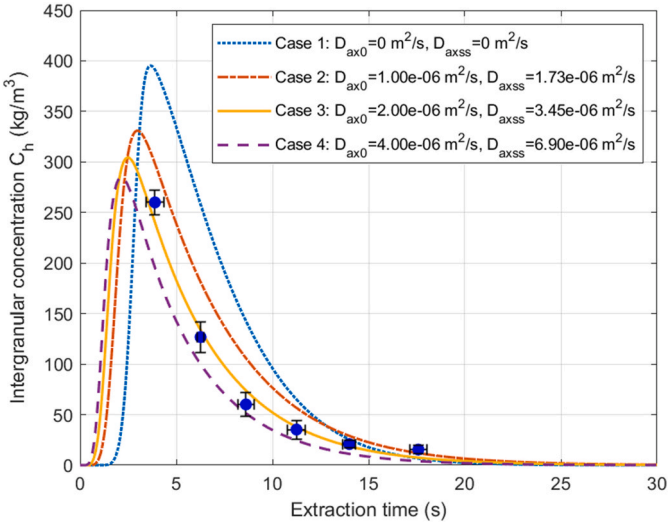

Fig. 13. Analytical case comparison of using different axial diffusion coefficients from the proposed model. Results were obtained using the fitted parameters from Table 6 for distribution A extracted TDS. With exception from D_{ax0} and D_{axss}, the rest of the parameters were kept constant, as presented in Tables 4 and 5.

As a second part of the analysis, an additional fitting of the parameters α*, β* and C_{sat} was performed for the three additional cases presented by employing the same conditions as for case 3 in the above sections. The results contained in Table 8, show that when the axial dispersion is neglected or is relatively smaller, the fitted values α* and β* may tend to capture the effect of the axial dispersion. This can be seen in case 1 and 2 where the filling phase time increases significantly due to a more plug flow behavior. The latter results in a considerably higher concentration during the first seconds of extractions. To compensate this, the fitted value α* decreased whereas β* increases aiming to achieve lower initial concentrations and a rapid decay. When the axial dispersion is increased in case 3 and 4, larger values of the parameter α* were found and at the same time relatively lower β* values. For all cases the C_{sat} tended to 513 kg/m3, which is the concentration inside the pores C_{V0}, set as a lower limit. The highest value for α* and a lowest value for β* were both found with case 4, due to the low initial concentrations from this case. Moreover, we deduce that the low initial concentrations actually measured in the experiments may be due to the large flow volume bypass effect, studied in other related works as caused by flow induced mechanical erosion (Mo et al., 2021). This effect is generally known as "channeling" in espresso extraction and can be described with the axial dispersion.

The best fitting results were then found for the higher axial dispersion coefficient case 3 and 4 with R^2 value of 0.99 and 0.90 (see Table 8). This fact indicates that taking into account the axial dispersion is crucial to describe the extracted concentration accurately with the proposed model, where the initial bed filling phase is considered.

4. Conclusions

The objective of this work was to characterize the dispersed axial water flow inside different coffee beds with similar extraction volume flow rates. The non-ideal flow through the bed was integrated in an existing coffee extraction model via an axial diffusion coefficient to predict instant concentrations of TDS and individual components at the bed exit. A tracer pulse method using KCl solution was applied. The Bodenstein number, hence the axial diffusion coefficient, were calculated from the obtained residence time distribution curves. Results indicated that the flow inside the bed cannot be considered as ideal, hence the obtained value of the axial diffusion coefficient was large enough not to be neglected. It was also found that the *Bo* number decreased up to a final average value as the extraction progressed, which may reflect the dynamic clogging effect of coffee beds identified in many other studies. This observed behavior was included in the model as an increase of the axial diffusion coefficient from the initial filling phase to the steady-state. The model was fitted to previously reported experiments using the lower limit particle size distribution with a mean diameter of the coarse volume fraction of $d_{4,3} = 325$ μm and similar extraction conditions as the non-ideal flow characterization experiments in this work.

From the validation results it was proven that the proposed approach is able to predict bed exit instant concentrations (for the total dissolved solids and the individual species) from beds with different size distributions in a range of $d_{4,3,} = 459$ μm–611 μm without the need to assume

Table 8
Results of fitting the proposed model using the different proposed cases of axial diffusion coefficients presented in Fig. 13. The fitting parameters are the α* and b* with their respective coefficient of determination R^2 from the fitting.

Distribution A	Case 1	Case 2	Case 3	Case 4
α* (−)	0.61	1.28	3.4	3.94
β* (−)	0.98	0.5	0.29	0.19
R^2	0.57	0.80	0.99	0.90

initial intergranular concentrations.

To improve the model, more precise information about the pore size distribution as function of mean particle size would be needed. Besides, experiments to determine the actual saturation concentration of the TDS and the individual components should be carried out. The latter could be integrated in the model in form of a partition coefficient. Moreover, a multicomponent mass transfer approach such as the one proposed by Taylor and Krishna (1993), could be followed to model the extraction of further espresso components. Finally, future studies will be focused in a more accurate determination of the bed axial dispersion, for instance using techniques such as in-situ microCT, to study the bed packed porosity evolution, thus the actual volume flow velocity inside the bed during extraction. The latter will also help to obtain more precise mass transfer coefficient values. This work proposes an approach to describe the dynamic filling phase during espresso extraction, where information about the actual flow behavior inside the bed is necessary.

CRediT authorship contribution statement

Mauricio Vaca Guerra: Conceptualization, Data curation, Formal analysis, Investigation, Methodology, Visualization, Writing - original draft, Writing - review & editing. **Yogesh M. Harshe:** Conceptualization, Methodology, Validation, Writing - review & editing. **Lennart Fries:** Conceptualization, Formal analysis, Methodology, Writing - review & editing. **James Payan Lozada:** Formal analysis, Investigation, Validation. **Aitor Atxutegi:** Conceptualization, Data curation, Investigation, Methodology, Validation, Writing - review & editing. **Stefan Palzer:** Project administration, Resources, Supervision. **Stefan Heinrich:** Formal analysis, Funding acquisition, Project administration, Supervision, Validation, Writing - review & editing.

Declaration of competing interest

The authors declare that they have no known competing financial interests or personal relationships that could have appeared to influence the work reported in this paper.

Data availability

Data will be made available on request.

Appendix

4.4 Full solution of the extraction model system of equations

The solution of the model system of equations include the parameters of bed intergranular concentration C_h, the intragranular concentration C_v, the particles porosity ε_{part} and the remaining volume fraction of TDS and individual species on the grains ψ. The solution also concerns the whole length of the discretized bed. The presented results of the instant concentrations at bed exit were taken from the last discretized layer from parameter C_h. Moreover, in this section, a complete analysis of the whole solution is included. Fig. 14 contains the solution for the parameters C_h and C_v as function of the extraction time and bed length respectively for the lower limit particle size distribution A. On the left hand side, the impact of the water filling phase of the bed can be directly seen; the intergranular concentration increases rapidly at the upper parts of the bed length first, as the water front advances towards the exit. The concentration differences across the bed length reaches a maximum value at around 3 s, which coincides with the bed exit time $t_{ext.}$ At this extraction point all the soluble mass which was rapidly transferred to the water front due to the initial large concentration difference is carried to the bottom of the bed. Henceforth, the concentrations C_v and C_h deviation decreases as the extraction progresses, tending to the same lower value after as the extraction time goes over 20 s. These results point out the importance of extracting long cups if the homogenous extraction of the bed is relevant.

The shoulder in the C_v concentration around 5s of extraction (see right hand side from Fig. 14) is strength correlated to the solution of the other two parameters of the model solution shown in Fig. 15. From the Figure can be seen that the total soluble solids are exhausted after circa 5s of extraction, leading to a considerably large increase of the bed intergranular concentration C_h. The mass transfer driving forces from the particles pores is therefore instantaneously reduced, which leads to a change in the decreasing trend of C_v.

Since it was assumed that all the soluble mass inside the pores was instantly dissolved as soon as the particles were reached by the water front, the particles porosity was then only impacted by the decrease of the remaining soluble coffee on the surface, dominated by the mass transfer coefficient β). The particles porosity ε_{part} increases rapidly at the upper layers of the bed to reach a final value at the same extraction time as the soluble coffee in the surface is depleted. The particle porosity increase is considerably lower towards the bottom layers of the bed; however also reaches the final value eventually. Further analysis could be made by comparing the behavior of these four intercorrelated parameters, for instance from the PSDs used for the model validation. Nonetheless, these insights are not included in this work.

4.5 Prediction of the final cup composition

The main goal of the extraction model, is to be able to predict the final cup composition. The total final cup volume is correlated to the extraction time via the average volume flow as follows:

$$V_{cup} = \frac{1}{\rho_{brew}} \int_{t_{exit}}^{t_{final}} \dot{m}\, dt \tag{A.1}$$

where t_{ext} (s) refers to extraction time at which the brew exited the bed after the filling phase and t_{final} (s) is the time point where the extraction was stopped. ρ_{brew} (kg/m^3) is the density, which was considered to be similar to pure water density and constant through all the extraction. The instant extracted mass of the brew can be determined as:

$$\dot{m} = Q\rho_{brew} \tag{A.2}$$

where Q (m^3/s) is the steady-state volume flow of the extraction. The cumulative extraction in the cup can be then obtained as the product of the total extracted mass of TDS or the corresponding individual component at t_{final}, and the final cup volume as follows:

$$m_{brew} = \int_{t_{exit}}^{t_{final}} \dot{m} C_i dt \tag{A.3}$$

where C_i (kg/m3) is the instant bed exit concentration at time *i*. Accordingly, the final cup concentration of TDS and the individual species is calculated with the cumulative extracted mass and the final volume of the cup:

$$C_{cup} = \frac{m_{brew}}{V_{cup}} \tag{A.4}$$

Note that in the calculation of this final cup parameter, the bed exit time t_{ext} refers to an approximation, obtained using the average mean time from Equation (2), which is approximately the time the water takes to cross the entire bed length at the averaged steady-state flow. However, as shown in the results of this work, the flow is relatively dispersed, which may lead to a non-homogenous exit of the brew after the initial filling phase. The latter could bring additional deviation between the predicted and the measured final cup concentration. Moreover, the comparison analysis of the calculated final concentrations and measured data are not included in this work.

Table 9
Obtained fitted parameters *a (m/s)* and *b (−)* from the exponential correlation between the calculated mass transfer coefficients α (m/s) and β (m/s) along with their respective coefficient of determination R^2 (−) for each fitting results respectively.

Mass transfer coefficient	*a (m/s)*	*b (−)*	R^2 (−)
α (m/s)	3.90×10^{-5}	0.07	0.62
β (m/s)	1.44×10^{-4}	0.13	0.83

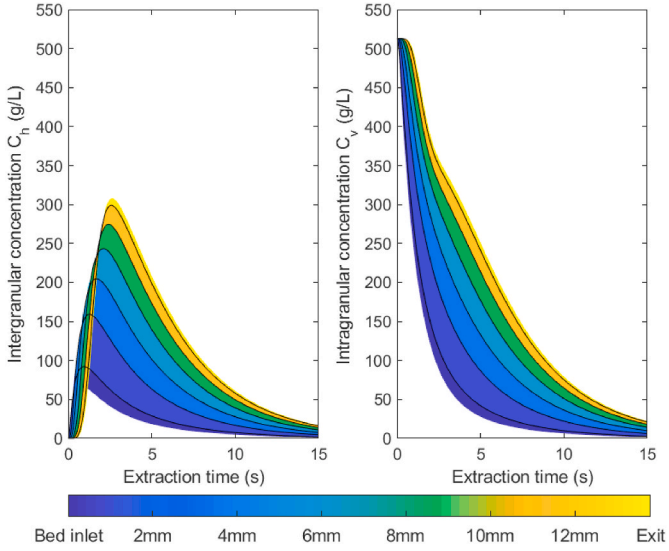

Fig. 14. Model solution for the intergranular concentration C_h (g/L) and intragranular concentration C_v (g/L) as function of the extraction time and the bed length, assumed to have a constant value of 13.4 mm.

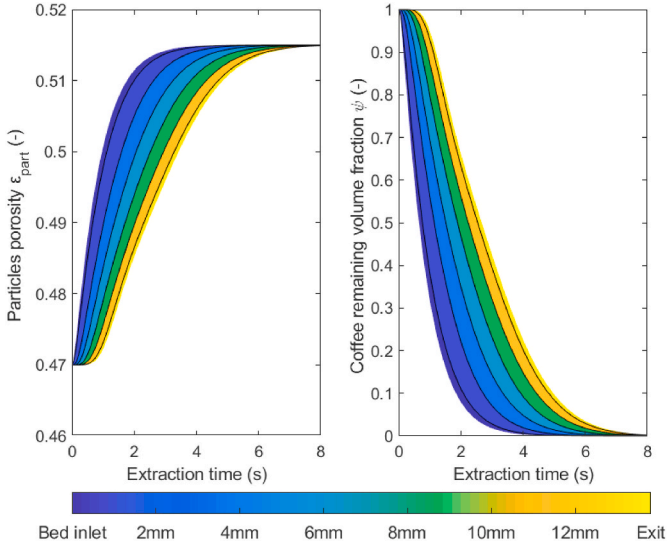

Fig. 15. Model solution for the particles porosity ε_{bed} (−) and the remaining coffee volume fraction at the particles surface ψ (−) parameters as function of extraction time (s) and bed length (mm), assumed to have a constant value of 13.4 mm.

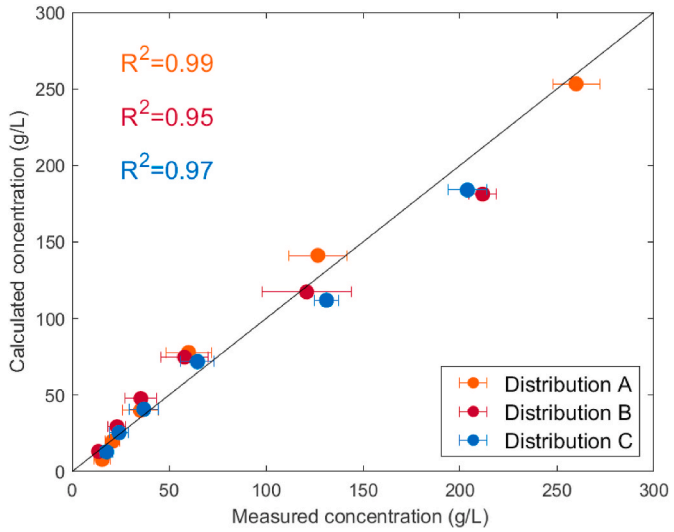

Fig. 16. Calculated and measured values of total dissolved solids (TDS) from experiments using distribution A, distribution B and distribution C.

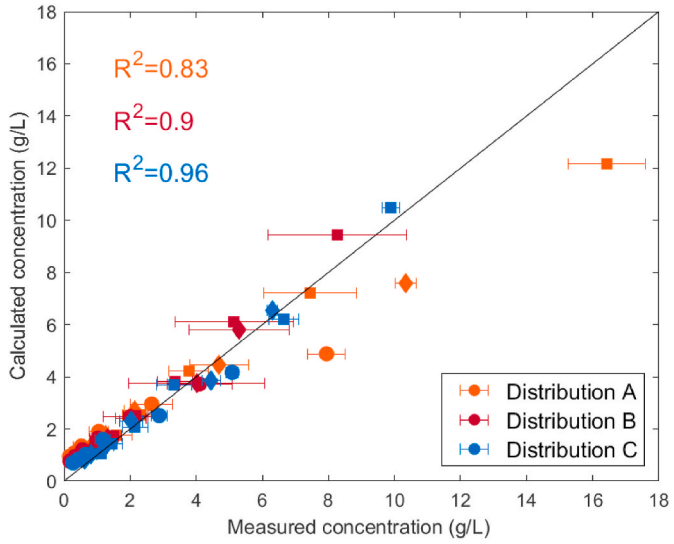

Fig. 17. Comparison of calculated and measured concentrations of trigonelline, caffeine and 5-CQA from experiments using distribution A, distribution B and distribution C.

Nomenclature

A	Total mass transport from particles pores term (kg/m^3 s)
B	Total mass transport from particles surface term (kg/m^3 s)
E(t)	Normalized E curve (1/s)
C_i	Instant concentration(kg/m^3)
C	Dimensionless concentration(−)
t_i	Measurement time (s)
u	Superficial flow velocity(m/s)
Bo	Bodenstein number(−)
D_{ax}	Axial dispersion coefficient(m^2/s)
D_{ax0}	Initial phase axial dispersion coefficient (m^2/s)
D_{axss}	Steady-state axial dispersion coefficient(m^2/s)
L	Length of the bed(m)
Q	Average steady state flow (m^3/s)
Y_{step}	Filling phase activation step (−)

Greek Symbols

σ	Residence time variance parameter (s^2)
α*	Fitting parameter mass transfer coefficient (−)
β*	Fitting parameter mass transfer coefficient (−)

α	Particles pores mass transfer coefficient (m/s)
β	Particles surface mass transfer coefficient (m/s)
ρ_{brew}	Density of the brew (kg/m^3)
θ	Dimensionless time(−)
C_{sat}	Saturation concentration(kg/m^3)
C_{v0}	Initial intraparticular concentration (kg/m^3)
C_{h0}	Initial interparticular concentration (kg/m^3)
C_h	Bed interparticular concencentration (kg/m^3)
X	Dimensionless length (−)
C_v	Intraparticular concentration (kg/m^3)
C_s	Coffee solid matrix density (kg/m^3)
m	Mean diameter of particle pores (m)
l	Coarse volume fraction diffusion length (m)
$\dot{m}$	Instant extracted mass (kg/s)
V_{cup}	Final volume cup (m^3)
r_s	Inverse value of φ_{s0}
m_{brew}	Cumulative extracted mass(kg)
C_{cup}	Final cup concentration(kg/m^3)
ψ	Remaining fraction of initial φ_{C0} (−)
φ_{c0}	Initial volume fraction of coffee/component in the grains (−)
φ_{s0}	Initial volume fraction of coffee/component in particles surface (−)
τ	Mean residence time (s)
ε_{bed}	Bed porosity (−)
ε_{part}	Particles porosity (−)

References

Alaqqad, M., Bennington, C.P.J., Martinez, D.M., 2012. An estimate of the axial dispersion during flow through a compressible wood-chip bed. Can. J. Chem. Eng. 90 (6), 1602–1611.

Anderson, B.A., Shimoni, E., Liardon, R., Labuza, T.P., 2003. The diffusion kinetics of carbon dioxide in fresh roasted and ground coffee. J. Food Eng. 59 (1), 71–78.

Arora, S., Potůček, F., 2009. Modelling of displacement washing of packed bed of fibers. Braz. J. Chem. Eng. 26 (2), 385–393.

Beverly, D., Lopez-Quiroga, E., Farr, R., Melrose, J., Henson, S., Bakalis, S., Fryer, P.J., 2020. Modeling mass and heat transfer in multiphase coffee aroma extraction. Ind. Eng. Chem. Res. 59 (24), 11099–11112.

Brodin, F.W., Sonavane, Y., Sedin, M., 2013. Displacement washing of TEMPO-oxidized softwood kraft pulp: effects of change in fiber properties. Nord. Pulp Pap Res. J. 28 (3), 366–376.

Cameron, M.I., Morisco, D., Hofstetter, D., Uman, E., Wilkinson, J., Kennedy, Z.C., Fontenot, S.A., Lee, W.T., Hendon, C.H., Foster, J.M., 2020. Systematically improving espresso: insights from mathematical modeling and experiment. Matter 2 (3), 631–648.

Corrochano, B.R., 2017. Advancing the Engineering Understanding of Coffee Extraction. Doctoral Dissertation. University of Birmingham, England.

Corrochano, B.R., Melrose, J.R., Bentley, A.C., Fryer, P.J., Bakalis, S., 2015. A new methodology to estimate the steady-state permeability of roast and ground coffee in packed beds. J. Food Eng. 150 (25), 106–116.

Danckwerts, P.V., 1953. Continuous flow systems. Distribution of residence times. Chem. Eng. Sci. 2 (1), 1–13.

Ellero, M., Navarini, L., 2019. Mesoscopic modelling and simulation of espresso coffee extraction. J. Food Eng. 263, 181–194.

Fries, L., 2021. Modeling food particle systems: a review of current progress and challenges. Annu. Rev. Chem. Biomol. Eng. 12, 97–113.

International Coffee Organization (ICO), 2021. Coffee Market Report-June 2021. (Accessed 31 July 2023).

Kuhn, M., Lang, S., Bezold, F., Minceva, M., Briesen, H., 2017. Time-resolved extraction of caffeine and trigonelline from finely-ground espresso coffee with varying particle sizes and tamping pressures. J. Food Eng. 206, 37–47.

Levenspiel, O., 1972. Chemical Reaction Engineering, second ed. ed. John Wiley & Sons, New York, pp. 258–259. 299.

Mo, C., Johnston, R., Navarini, L., Ellero, M., 2021. Modeling the effect of flow-induced mechanical erosion during coffee filtration. Phys. Fluids 33 (9).

Mo, C., Navarini, L., Liverani, F.S., Ellero, M., 2022. Modeling swelling effects during coffee extraction with smoothed particle hydrodynamics. Phys. Fluids 34 (4), 43104.

Moroney, K.M., Lee, W.T., Suijver, F., Marra, J., 2015. Modelling of coffee extraction during brewing using multiscale methods: an experimentally validated model. Chem. Eng. Sci. 137, 216–234.

National Center for Biotechnology Information, 2022. PubChem Compound Summary. (Accessed 20 July 2023).

Potůček, F., Miklík, J., 2010. Displacement washing of kraft pulp cooked from a blend of hardwoods. Chem. Pap. 64 (2).

Reynolds, W., 2019. Modeling and scale-up of hydrothermal pretreatment in compressible lignocellulosic biomass fixed-beds with changing properties. Dissertation, Verlag Dr. Hut; Technische Universität Hamburg.

Reynolds, W., Singer, H., Schug, S., Smirnova, I., 2015. Hydrothermal flow-through treatment of wheat-straw: detailed characterization of fixed-bed properties and axial dispersion. Chem. Eng. J. 281 (3), 696–703.

Schenker, S., Handschin, S., Frey, B., Perren, R., Escher, F., 2000. Pore structure of coffee beans affected by roasting conditions. J. Food Sci. 65 (3), 452–457.

Schmieder, Benedikt K.L., Pannusch, Verena B., Vannieuwenhuyse, Lara, Briesen, Heiko, Minceva, Mirjana, 2023. Influence of flow rate, particle size, and temperature on espresso extraction kinetics. In Foods 12 (15), 2871.

Spiro, M., Selwood, R.M., 1984. The kinetics and mechanism of caffeine infusion from coffee: the effect of particle size. J. Sci. Food Agric. 35 (8), 915–924.

Taylor, R., Krishna, R., 1993. Multicomponent Mass Transfer. John Wiley & Sons.

Vaca Guerra, M., Harshe, Y.M., Fries, L., Pietsch-Braune, S., Palzer, S., Heinrich, S., 2023a. Tuning the packed bed configuration for selective extraction of espresso non-volatiles based on polarity. J. Food Eng. 354, 111554.

Vaca Guerra, M., Harshe, Y.M., Fries, L., Rothberg, S., Palzer, S., Heinrich, S., 2023b. Influence of particle size distribution on espresso extraction via packed bed compression. J. Food Eng. 340 (5–6), 111301.

Wang, X., William, J., Fu, Y., Lim, L.T., 2016. Effects of capsule parameters on coffee extraction in single-serve brewer. Food Res. Int. 89 (Pt 1), 797–805.